OPTIMIZING OPTICAL NONLINEARITIES IN GaInAs/AlInAs QUANTUM CASCADE LASERS

by

Aleksandra GAJIĆ [1,2]***, Jelena RADOVANOVIĆ*** [3*]***, Vitomir MILANOVIĆ*** [3]***, Dragan INDJIN*** [4]***, and Zoran IKONIĆ*** [4]

[1]School of Electrical Engineering, University of Belgrade, Belgrade, Serbia
[2]Telekom Serbia, Belgrade, Serbia
[3]Faculty of Electrical Engineering, University of Belgrade, Belgrade, Serbia
[4]School of Electronic and Electrical Engineering, University of Leeds, Leeds, UK

Scientific paper
DOI: 10.2298/NTRP1401000G

Regardless of the huge advances made in the design and fabrication of mid-infrared and terahertz quantum cascade lasers, success in accessing the ~3-4 μm region of the electromagnetic spectrum has remained limited. This fact has brought about the need to exploit resonant intersubband transitions as powerful nonlinear oscillators, consequently enabling the occurrence of large nonlinear optical susceptibilities as a means of reaching desired wavelengths. In this work, we present a computational model developed for the optimization of second-order optical nonlinearities in $In_{0.53}Ga_{0.47}As/Al_{0.48}In_{0.52}As$ quantum cascade laser structures based on the implementation of the genetic algorithm. Carrier transport and the power output of the structure were calculated by self-consistent solutions to the system of rate equations for carriers and photons. Both stimulated and simultaneous double-photon absorption processes occurring between the second harmonic generation-relevant levels are incorporated into rate equations and the material-dependent effective mass and band non-parabolicity are taken into account, as well. The developed method is quite general and can be applied to any higher order effect which requires the inclusion of the photon density equation.

Key words: quantum cascade laser, genetic algorithm, second harmonic generation, optical nonlinearity

INTRODUCTION

Quantum cascade lasers (QCL) represent a class of semiconductor injection lasers based on intersubband transitions in multiple quantum well (QW) structures. The vast number of QW that form these structures, which can be measured in hundreds, allow us the flexibility of tailoring various output properties to demand, in accordance with or even optimized for a particular application, by simply modifying the thickness and/or composition of the constituent layers [1, 2]. In the past couple of years this design flexibility has expanded the achievable wavelength range from 3-25 μm to the terahertz regime, which, together with the ability of room temperature operation, has marked these lasers as practical and reliable light sources for a variety of applications such as trace chemical sensing, health monitoring and infrared countermeasures [3-10].

Besides the linear optical properties, resonant intersubband transitions can also be utilized for strong nonlinear effects, enabling huge nonlinear optical susceptibilities to take place [11]. These optical nonlinearities can have a vast range of possible applications, due to the capability of changing the frequency of the fundamental laser source [12, 13].

A necessary requirement for effective QCL design is acknowledging all the physical processes that occur in the active laser region of these complex devices, as well as creating a systematic and precise modeling technique which will be able to successfully reproduce them. This makes the inclusion of all relevant scattering mechanisms that take place in both the optically active and collector(extractor)/injector multi-quantum well regions of the QCL essential for an accurate description of carrier dynamics [14, 15].

In the work presented here, we will address the optimization of two-QW active region mid-infrared (MIR) QCL [16] with respect to resonant second-order susceptibility ($\chi^{(2)}$). The optimal potential profile that maximizes the product of dipole matrix elements relevant to $\chi^{(2)}$ associated with the second harmonic generation (SHG) is obtained by employing the genetic algorithm.

* Corresponding author; e-mail: radovanovic@etf.bg.ac.rs

The output properties of the optimized structure are calculated by using the full self-consistent rate equation model which includes both carrier and photon densities [5, 17], while the results of the calculations predict a noticeable improvement of the targeted nonlinear optical susceptibility and, consequently, of the nonlinear output power for the optimized design.

THEORETICAL CONSIDERATIONS

Active region optimization

Optimization through mathematical modeling has been utilized in many applications [18], and probably the most promising one is its deployment in the field of improvement of the output characteristics of heterostructure-based devices [19, 20]. There are several techniques that can be applied for solving this particular problem [21] and in this work we have adopted a global optimization technique based on the use of the genetic algorithm [22]. This algorithm belongs to a larger class of evolutionary algorithms and represents a search heuristic used to generate solutions to optimization and search problems by a combination of selection, recombination and mutation [23, 24], actually mimicking processes that occur in nature. It is chosen for its ability to address problems that standard optimization algorithms cannot handle, *i. e*. entailing objective functions which are discontinuous, non-differentiable, stochastic, or highly nonlinear. Also, unlike other techniques in use, the genetic algoritham (GA) can be easily adapted so that it takes into account various design constraints, such as supersymetric quantum mechanics, which will produce a smooth potential profile that requires additional discretization.

Due to their extremely complex structure and a large number of parameters to be considered, the optimization of the entire QCL structure would be highly demanding, so we have focused on the optimization of the active region which we then seamlessly assimilate with the existing injector/collector design.

Typically, active regions in MIR QCL consist of a minimum of three consecutive energy levels, with the radiative transitions occurring between the upper and lower laser levels, while the electrons quickly leave the lower laser level by resonant LO phonon scattering into the first, basic, level of the active region. However, a QCL structure capable of second harmonic generation contains one more significant energy triplet in which at least one energy level needs to be populated with free electrons in order for the structure to be able to generate radiative transitions and act as an efficient nonlinear converter. This sets an important design requirement, *i. e*. that the upper laser level needs to coincide with one of the levels in the nonlinear cascade.

In our optimization model, we start with the existing design (see [16]) in which the active region consists of two coupled InGaAs quantum wells separated with an AlInAs barrier. The optimization target function is chosen so as to maximize the second order nonlinear susceptibility [25]

$$\chi^{(2)}(2\omega) \approx \approx \frac{2\pi e^3}{d\varepsilon_0}\left[\frac{M_{23}M_{34}M_{24}}{\gamma_{42}}\left(\frac{n_3-n_4}{\gamma_{43}}+\frac{n_3-n_2}{\gamma_{32}}\right)+ +\frac{M_{34}M_{45}M_{35}}{\gamma_{53}}\left(\frac{n_4-n_5}{\gamma_{53}}+\frac{n_4-n_3}{\gamma_{43}}\right)\right] \quad (1)$$

where, M_{ij} is the dipole matrix element between levels i and j, γ_{ij} – the full width half maximum for transitions occurring between levels i and j, n_i – the sheet electron density of level i, and d represents the layers width.

Taking into account that $n_3 \gg n_4, n_5$, as well as that the γ_{ij} have similar values [16], the following relevant quantity for optimization may be extracted from eq (1).

$$F_T = \left| M_{34} n_3 \left[M_{23} M_{24} \left(2 - \frac{n_2}{n_3} \right) - M_{45} M_{35} \right] \right| \quad (2)$$

The optimization is performed for a fixed external field value, with the objective to maximize the function F_T, eq. (2), by varying the constituent layer thicknesses which form the parameter vector. At the same time, several constraints need to be addressed. Transition energies, ΔE_{21} and ΔE_{32}, defined by the LO phonon and transition energy, respectively, together with the transition energies between the levels constituting the cascades, ΔE_{54} and ΔE_{43}, should remain unchanged. The layer thicknesses are only allowed to have non-negative values, and these are limited to 105 Å (1Å = 10^{-10} m) for the wells and 30 Å for the barriers. Additional constraints concern the minimal value of the matrix element, as well as the upper laser level energy which is set to fit the injector region. Also, the limitation regarding the favoring of diagonal transitions in order to increase the upper laser level lifetime must be carefully balanced with the constraint regarding the matrix element, making the optimization process extremely difficult and complex.

The design process is concluded by adding the existing injector/collector region.

The self-consistent rate equation model

The output characteristics are calculated by applying the full self-consistent rate equation modeling of electron transport [14] to the optimized structure. The model includes photon density equations describing single- and double-photon stimulated emission processes which significantly increase the complexity of the numerical procedure.

In the model applied in this calculation, we can use a simplified form of the model described in [26, 27], in which the number of relevant energy levels is restricted to five per QCL region (five in the optically active region and five in each injector and collector/extractor regions), see fig. 2. Adopting the notation and subband indexes given in [26], the injector and collector regions are represented with five energy levels each, subbands 1, 2, 3, 5, and 7 in the collector, and 8, 10, 11, 13, and 15 in the injector. Active region levels 14, 12, 9, and 6 are equally spaced with the energy intervals resonant to the lasing frequency. Level 4 represents the active region ground state which is located one LO phonon energy below the lower laser level (6), so as to facilitate faster carrier extraction from the active QCL region into the following collector/injector region of the subsequent period, see fig. 2.

If we make the assumption that the transitions between the injector and collector are negligible, the rate equation for subband 1 can be written as

$$\frac{\mathrm{d}n_1}{\mathrm{d}t} = \sum_j (W_{j1} n_j + W_{j8} n_j - W_{1j} n_1 + W_{8j} n_8) + \sum_k (W_{k1} n_k - W_{1k} n_1) \tag{3}$$

where, W_{pq} represents the total scattering rate between subbands p and q. In the equation above, indexes j and k are equal to $j = 4, 6, 9, 12$, and 14 and $k = 2, 3, 5$, and 7, while similar equations can be written for all other injector/collector states.

In the case of active region levels 4, 6, 9, 12, and 14, the rate equation is given by

$$\frac{\mathrm{d}n_j}{\mathrm{d}t} = \sum_{i=1, i\neq j}^{15} (W_{ij} n_i - W_{ji} n_j) \tag{4}$$

where $j = 4, 6, 9, 12$, and 14.

The contribution of SHG resonant levels, *i. e*., 6-9-12 and 9-12-14 cascades, is reflected through both sequentially and simultaneously resonant intracavity double-photon processes. The incorporation of these processes into the rate equation model is essential, since the two-photon absorption between 9 and 14 and emission between levels 12 and 6 can seriously influence the lasing performance, due to the reduced population inversion between lasing states 6 and 9. They are taken into account by extending the rate equations system with the rate equation for the density of photons describing single- and double-photon stimulated emission processes

$$\frac{\mathrm{d}m_\omega}{\mathrm{d}t} = \frac{\Gamma}{d}[W^p_{96}(n_9 - n_6) + W^p_{(14)(12)}(n_{(14)} - n_{(12)}) + W^p_{(12)9}(n_{(12)} - n_9)] + 2\frac{\Gamma}{d}[W^{2p}_{(14)9}(n_{(14)} - n_9) + W^{2p}_{(12)6}(n_{(12)} - n_6)] - \frac{m_\omega}{\tau^\omega_p} \tag{5}$$

here, m_ω is the photon density [m^{-3}], W^p_{ij} and W^{2p}_{ik} are the single- and double-photon stimulated emission rates, Γ – the mode confinement factor assumed to be 0.5 [28], and τ^ω_p – the photon lifetime related to the total loss α_ω as [28] $\tau^\omega_p = (v_g \alpha_\omega)^{-1}$, where v_g represents group velocity, $v_g = c/n_\omega$.

The single-photon stimulated emission rate is expressed as [29]

$$W^p_{ij} = \frac{e^2 M^2_{ij} \omega}{2\varepsilon} \frac{\gamma_{ij}}{(E_{ij} - \hbar\omega)^2 + \left(\frac{\gamma_{ij}}{2}\right)^2} m_\omega \tag{6}$$

where, E_{ij} is the energy difference between levels i and j, ε – the permittivity of the lasing medium and ω – the incident photon frequency. It can be seen from the expression eq. (6) that the single-photon stimulated emission rate is proportional to incident photon density (light intensity). The double-photon stimulated emission/absorption rate in the transition cascade *i-j-k* is proportional to the photon density squared, as given in [16, 28]

$$W^{2p}_{ik} = \frac{e^4 M^2_{ij} M^2_{jk}}{4\hbar\varepsilon^2} \left(\frac{\hbar\omega}{E_{jk} - \hbar\omega}\right) \cdot \frac{\gamma_{ik}}{(E_{ik} - 2\hbar\omega)^2 \left(\frac{\gamma_{ik}}{2}\right)^2} m^2 \omega \tag{7}$$

In addition, in the rate equations system described by eqs. (3) and (4) , the total scattering rates between any two levels of the nonlinear cascade in the active region include not only the nonradiative scattering rates originating from electron-LO phonon and electron-electron scattering, but also from the radiative single- and two-photon transitions which are linearly and/or quadratically dependent on the incident photon density.

For any other transitions occurring outside the active region, scattering rates are obtained by taking into account electron-LO phonon and electron-electron scattering only, making these transitions independent of the photon density in the cavity.

The set of equations expressed by eqs. (3) and (4) , together with eq. (5) describing the photon density, form a total of 16 rate equations whose solution for electron and photon densities n_i and m_ω, respectively, can enable us to estimate macroscopic parameters of the system, such as the linear and nonlinear output power. The scattering time $W_{i,f}$ is a function of both n_i and n_f – initial and final subband populations, as well as of photon density, as stated in eqs. (6) and (7), hence the set of equations needs to be solved self-consistently, using an iterative procedure [14, 26].

Linear and SHG output light intensity can be calculated from the photon density in the cavity as

$$I_\omega = N_{\mathrm{mod}}(\hbar\omega) m_\omega \frac{c}{n_\omega} \tag{8}$$

where, N_{mod} is the number of QCL periods in the lasing cavity, set to 50 as in [16], while factor c/n is the speed of light in the lasing cavity. The output power can now be calculated as

$$P_{\omega} = I_{\omega} A \tag{9}$$

where, A represents the cross-sectional area transverse to the light propagation direction.

By solving the steady-state rate equations system given by eqs. (3)-(5), we can determine the photon density and, correspondingly, the initial fundamental power output given by eqs. (8) and (9). The nonlinear output power can then be obtained from the following expression [28, 29]

$$P_{2\omega} = \frac{2\pi^2 |\chi^{(2)}|^2 (1-R_2)}{I_R n_{\omega}^2 n_{2\omega} \lambda^2 c\varepsilon_0 (1-R_1)^2} \cdot \frac{e^{-2\alpha_{2\omega}L} - 2e^{-2\alpha_{2\omega}L}\cos(\Delta kL) + 1}{\Delta k^2 + \alpha_{2\omega}^2} P_{\omega}^2 \tag{10}$$

here, $\lambda \sim 9$ μm is the wavelength of the fundamental mode and IR represents the effective interaction cross section decided by the overlap between the fundamental and the second harmonic mode, considered to be equal to the one given in [16], *i. e.* 1000 μm^2. $n_{\omega} = k_{\omega}c/\omega$ and $n_{2\omega} = k_{2\omega}c/\omega$ are refractive indices of the fundamental and second harmonic mode, $\Delta k = 2k_{\omega} - k_{2\omega}$ the phase constant mismatch and $\alpha_{2\omega}$ is the total loss including both the waveguide $\alpha_{2\omega}^{\omega}$ and the mirror loss $\alpha_{2\omega}^{m}$. The waveguide losses, as well as the dimensions of the waveguide, are taken from [16]. The mirror losses can be estimated by

$$\alpha_{\omega(2\omega)}^{m} = \frac{-(\ln R_{1(2)})}{L} \tag{11}$$

where, L is the cavity length, while R_1 and R_2 are reflection coefficients at the fundamental and second harmonic frequency. They are related to the refractive indices as

$$R_{1(2)} = \frac{(1-n_{\omega(2\omega)})^2}{(1+n_{\omega(2\omega)})^2} \tag{12}$$

The macroscopic parameters of the system, such as linear and SHG power, can be evaluated by repeating the self-consistent procedure for a number of external fields and by calculating the lifetimes and transition matrix elements which, consequently, influence the electric current and subband populations, as well as photon density.

NUMERICAL RESULTS AND DISCUSSION

The previously described procedure is flexible and widely applicable to any number of structures. However, here we have chosen to consider the optimization of the active region for the reference structure described, [16], which consists of two coupled InGaAs quantum wells separated by an AlInAs barrier, designed for fundamental and SHG wavelengths at $\lambda \sim 9$ μm and $\lambda \sim 4.5$ μm, respectively. This limits the fundamental transition energy to approximately 136 meV, while the energy difference between the ground and the lower laser level is defined by LO phonon energy and amounts to 34 meV. The optimization was carried out for the value of the applied field of $F = 38$ kV/cm, temperature $T = 10$ K, and sheet carrier density $N_s = 37.2 \cdot 10^{10}$ cm^{-2}, which was derived from the dopant profile per repeat period and was, initially, at the beginning of the self-consistent procedure, assumed to be distributed equally between the subbands of one period.

In order to better illustrate the iterative procedure described in the previous chapter, the result of the self-consistent calculation for one of the parameters, namely photon density, is shown in fig. 1. The time interval for solving the differential equations is set to 1 ps, the value reaching convergence after approximately 30 iterations, while the number of iterations differs from structure to structure and is not the same for the reference and the optimized structure.

A schematic diagram of quasi-bound energy levels and associated wave functions squared for an injector-active region-injector section of the optimized structure is shown in fig. 2. The layer sequence of one period, in nanometers, starting from the injection barrier is: **4.1**, 8.6, **1.5**, 5.7, **2.6**, 4.1, **2.1**, 3.9, **2.3**, 3.7, **2.5**, 3.5, **2.6**, and 3.3, where normal scripts denote the wells and bold the barriers. The injector and collector regions are numbered, as given in the previous paragraph. Nonlinear cascades are formed by levels 6-9-12 and 9-12-14. The first cascade coincides with the laser transition, while the resonance of the second cascade can be achieved by relative thickness variations of the two QW and the barrier between them. At the applied

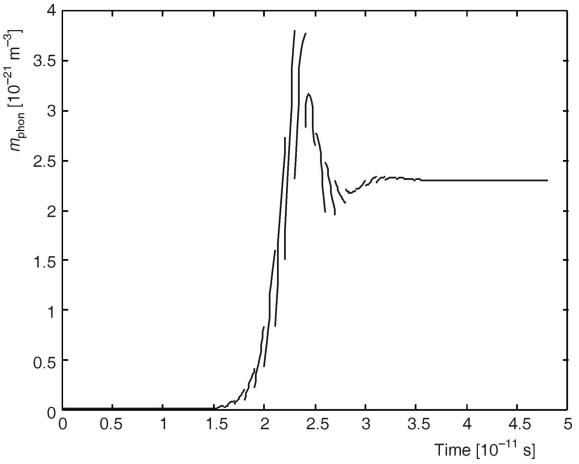

Figure 1. The result of the self-consistent calculation for photon density. The time interval for solving the differential equations is set to 1 ps; as can be seen, the value reaches convergence after approximately 30 iterations

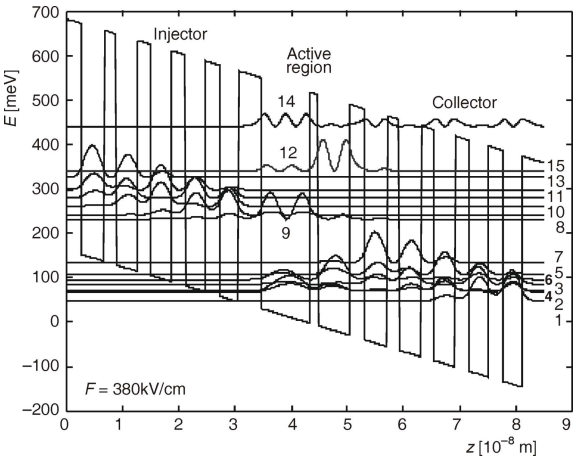

Figure 2. A schematic diagram of quasi-bound energy levels and associated wave functions squared for one and a half period of the optimized structure. The layer sequence of one period, in nanometers, starting from the injection barrier is: *4.1*, 8.6, *1.5*, 5.7, *2.6*, 4.1, *2.1*, 3.9, *2.3*, 3.7, *2.5*, 3.5, *2.6*, and 3.3. Normal bold scripts denote the wells and bold italic the barriers

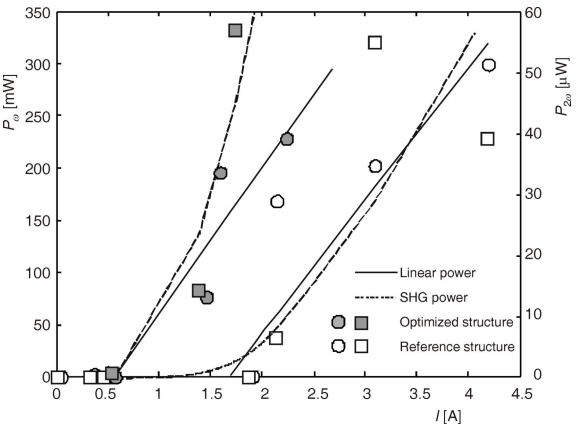

Figure 3. Fundamental power (straight line) and the nonlinear power (dashed line) under different pump currents for the optimized (grey symbols) and reference (white symbols) structure. The lines represent interpolated values of the calculated data which are denoted by symbols (squares and circles)

bias field of 38 kV/cm, for which the optimization was performed, the lasing wavelength amounts to $\lambda = 9.08\ \mu$m.

By using eq. (10) and adopting the parameters given in [16], we can estimate the nonlinear conversion efficiency $\eta = P_{2\omega}/P_{\omega}^2$ of 272 μW/W^2 for the reference structure, which is in good agreement with the experimentally obtained values of ~100 μW/W^2 given in [16]. The calculated value for the second order nonlinear susceptibility of $|\chi^{(2)}| = 2.58 \cdot 10^4$ pm/V is in accordance with the calculated values of $2 \cdot 10^4$ pm/V given for the reference structure in [16]. However, the optimized structure shows a noticeable improvement regarding these parameters and the calculated values for the nonlinear-to-linear conversion efficiency and the second-order nonlinear susceptibility are 349 μW/W^2 and $2.71 \cdot 10^4$ pm/V, respectively.

Figure 3 represents the linear and nonlinear output for both the reference and the optimized structure. The calculated values are represented with symbols: white for the reference structure [16] and grey for the optimized one. Circles correspond to the linear, squares to SHG power. The threshold current estimated for the optimized structure is close to 0.5 A, while the calculated value for the reference structure is about 2 A, which is in good accordance with the experimentally obtained values given in [16]. It can be seen that the optimized structure shows higher linear output powers at lower currents.

As can be seen from eq. (10), the phase mismatch factor Δk plays a significant role in nonlinear conversion efficiency estimation. In our calculations, the phase mismatch factor is about 100 times larger than the loss $\alpha_{2\omega}$. Even though the calculated values for the nonlinear conversion efficiency are rather high, they could be additionally enhanced by making the phase mismatch factor comparable to the optical losses, or by decreasing the effective interaction area I_R, which will be the subject of further work.

CONCLUSIONS

A procedure for the design and optimization of a GaInAs-AlInAs-based QCL is proposed. It relies on the use of the Genetic Algorithm for the purpose of determining a set of design parameters that would facilitate large nonlinear optical susceptibilities. The described technique was applied to the optimization of a double quantum well laser and the output characteristics of both; the reference structure and the optimized structure were evaluated by modeling the carrier dynamics by use of the full self-consistent approach extended with photon density equations. Reference design calculations show excellent agreement with experimental results while, simultaneously, the optimized structure predicts a significant improvement of the nonlinear-to-linear conversion efficiency and the second-order nonlinear susceptibility, as intended.

The technique has no restrictions regarding the number of optimization parameters or material composition and demonstrates high optimization abilities.

ACKNOWLEDGMENTS

This work was supported by the Ministry of Education, Science and Technological Development (Republic of Serbia), ev. no. III 45010, NATO SfP Grant, ref. no. 984068, and COST Actions BM1205 and MP1204.

AUTHOR CONTRIBUTIONS

The theoretical analysis was carried out by A. Gajić, J. Radovanović, and V. Milanović. Numerical calculations were performed by A. Gajić. All authors analysed and discussed the results. The manuscript was written by A. Gajić and J. Radovanović and the figures prepared by A. Gajić.

REFERENCES

[1] Radovanović, J., *et al*., Influence of the Active Region Design on Output Characteristics of Gaas/Algaas Quantum Cascade Lasers in a Strong Magnetic Field, *Semicond. Sci. Technol., 21* (2006), 3, pp. 215-220
[2] Höfling, S., *et al*., Dependence of Saturation Effects on Electron Confinement and Injector Doping in GaAs/$Al_{0.45}Ga_{0.55}As$ Quantum-Cascade Lasers, *Appl. Phys. Lett., 88* (2006), 25, pp. 1109-1111
[3] Wlliams, B. S., Terahertz Quantum-Cascade Lasers, *Nat. Photonics, 1* (2007), pp. 517-525
[4] Yao, Y., Hoffman, A. J., Gmachl, C. F., Mid-Infrared Quantum Cascade Lasers, *Nat. Photonics, 6* (2012), pp. 432-439
[5] Petitjean, Y., *et al*., Dynamic Modeling of Terahertz Quantum Cascade Lasers, *Sel. Top. Quantum Electron., 17* (2011), 1, pp. 22-29
[6] Capasso, F., *et al*., Quantum Cascade Lasers: Ultrahigh-Speed Operation, Optical Wireless Communication, Narrow Linewidth, and Far-Infrared Emission, *IEEE J. Quant. Electron., 38* (2002), 6, pp. 511-532
[7] Sirtori, C., *et al*., GaAs/AlGaAs Quantum Cascade Lasers, *Appl. Phys. Lett., 73* (1998), 24, pp. 3486-3488
[8] Sirtori, C., Page, H., Becker, C., GaAs-Based Quantum Cascade Lasers, *Proc. R. Soc. London, Ser., A 359* (2001), pp. 505-522
[9] Lee, S. C., Wacker, A., Nonequilibrium Green's Function Theory for Transport and Gain Properties of Quantum Cascade Structures, *Phys. Rev., B 66* (2002), 24, pp. 245314-245332
[10] Radovanović, J., Milanović, V., Quantum Cascade Laser: Applications in Chemical Detection and Environmental Monitoring, *Nucl Technol Radiat, 24* (2009), 2, pp. 75-81
[11] Belkin, M. A., *et al*., Terahertz Quantum-Cascade-Laser Source Based on Intracavity Difference-Frequency Generation, *Nature Photonics, 1* (2007), pp. 288-292
[12] Belkin, M. A., *et al*., Room Temperature Terahertz Quantum Cascade Laser Source Based on Intracavity Difference-Frequency Generation, *Appl. Phys. Lett., 92* (2008), 20, pp. 1101-1104
[13] Bengloan, J. Y., *et al*., Intracavity Sum-Frequency Generation in Gaas Quantum Cascade Lasers, *Appl. Phys. Lett., 84* (2004), 12, pp. 2019-2022
[14] Mirčetić, A., *et al*., Towards Automated Design of Quantum Cascade Lasers, *J. Appl. Phys., 97* (2005), 8, pp. 4506-4513
[15] Novaković, B., *et al*., Influence of Electron-Electron Scattering on Electron Relaxation Rates in Three and Four-Level Quantum Cascade Lasers in Magnetic Fields, *Opt. Comm., 279* (2007), 2, pp. 330-335
[16] Gmachl, C., *et al*., Optimized Second-Harmonic Generation in Quantum Cascade Lasers, *IEEE J. Quantum Electron., 39* (2003), 11, pp. 1345-1355
[17] Hugi, A., Maulini, R., Faist, J., External Cavity Quantum Cascade Laser, *Semicond. Sci. Technol., 25* (2010), 8, pp. 083001-083006
[18] Plećaš, I., Nadjdjerdj, L.J., Davidović, M. D., Optimization by Mathematical Modeling of Physicochemical Characteristics of Concrete Containers in Radioactive Waste Management, *Nucl Technol Radiat, 28* (2013), 1, pp. 25-30
[19] Indjin, D., *et al*., Gain-Maximized GaAs/AlGaAs Quantum-Cascade Laser with Digitally Graded Active Region, *Appl. Phys. Lett., 81* (2002), 12, pp. 2163-2165
[20] Tomić, S., *et al*., The Optimization of Optical Gain in the Intersubband Quantum Well Laser, *J. Appl. Phys., 87* (2000), 11, pp. 7965-7972
[21] Smiljanić, J., *et al*., MATLAB-Based Program for Optimization of Quantum Cascade Laser Active Region Parameters and Calculation of Output Characteristics in Magnetic Field, *Comput. Phys. Commun*., (2013), http://dx.doi.org/10.1016/j.cpc.2013.10.025
[22] Daničić, A., *et al*., Optimization and Magnetic-Field Tunability of Quantum Cascade Laser for Applications in Trace Gas Detection and Monitoring, *J. Phys., D 43* (2010), 4, p. 04510
[23] Goldberg, D. E., Genetic Algorithms in Search, Optimization and Machine Learning, Addison-Wesley, Boston, Mass., USA, 1989
[24] Carroll, D. L., University of Illinois, Fortran Genetic Algorithm Driver, http://cuaerospace.com/carroll/ga.html
[25] Bai, J., Citrin, D. S., Supersymmetric Optimization of Second- Harmonic Generation in Mid-Infrared Quantum Cascade Lasers, *Opt. Expr., 14* (2006), 9, pp. 4043-4048
[26] Indjin, D., *et al*., Self-Consistent Scattering Theory of Transport and Output Characteristics of Quantum Cascade Lasers, *J. Appl. Phys., 91* (2002), 11, pp. 9019-9026
[27] Jovanović, V. D., *et al*., Influence of Doping Density on Electron Dynamics in GaAs/AlGaAs Quantum Cascade Lasers, *J. Appl. Phys., 99* (2006), 10, pp. 3106-3114
[28] Bai, J., Citrin, D. S., Optical and Transport Characteristics of Quantum-Cascade Lasers with Optimized Second-Harmonic Generation, *IEEE J. of Quant. Electron., 43* (2007), 5, pp. 391-398
[29] Boyd, R. W., Nonlinear Optics, 2nd ed., San Diego, Cal., USA, Academic, 2003, p. 528

Received on January 28, 2014
Accepted on February 14, 2014

Александра ГАЈИЋ, Јелена РАДОВАНОВИЋ, Витомир МИЛАНОВИЋ, Драган ИНЂИН, Зоран ИКОНИЋ

ОПТИМИЗАЦИЈА ОПТИЧКИХ НЕЛИНЕАРНОСТИ У GaInAs/AlInAs КВАНТНО КАСКАДНИМ ЛАСЕРИМА

Без обзира на огроман напредак остварен у области дизајна и израде квантно каскадних ласера прилагођених за зрачење у средње инфрацрвеној и терахерцној области спектра, опсегу таласних дужина од ~3-4 mm и даље се приступа са ограниченим успехом. Ова чињеница је довела до потребе да се резонантни унутарзонски прелази искористе као снажни нелинеарни осцилатори, што омогућава да се велике нелинеарне оптичке сусцептибилности искористе као средство за постизање жељене таласне дужине. У овом раду, представљамо рачунски модел за оптимизацију оптичких нелинеарности другог реда у $In_{0.53}Ga_{0.47}As/Al_{0.48}In_{0.52}As$ квантним каскадним ласерима заснован на примени генетског алгоритма. Транспортне карактеристике и излазна оптичка снага израчунати су самосагласним решавањем система брзинских једначина за електроне и фотоне. И стимулисани и спонтани дво и једно-фотонски процеси апсорпције који се јављају нивоа релевантних за генерацију другог хармоника су унети у брзинске једначине, а у обзир су узете и зонска непараболичност и зависност ефективне масе од материјала. Развијена метода је прилично општа и може се применити на било који ефекат вишег реда која захтева укључивање фотонске једначине.

Кључне речи: квантно каскадни ласер, генетски алгоритам, генерација другог хармоника, оптичка нелинеарност